Modified ginkgo leaves for adsorption of methyl violet and malachite green dyes in their aqueous system

Lincai Peng[a], Jing Gao[a], Shun Yao[a], Xianqiu Lan[a], Huaiping Li[b],*, Hang Song[a],*

[a]School of Chemical Engineering, Sichuan University, Chengdu 610065, China, Tel. +86-028-85405222;
emails: hangsong@vip.sina.com (H. Song), lincai.peng@foxmail.com (L. Peng), 1248381392@qq.com (J. Gao),
cusack@scu.edu.cn (S. Yao), 13699006688@163.com (X. Lan)
[b]Institute of Biology National Institute of Measurement and Testing Technology, Chengdu 610021, China,
Tel. +86-028-84403292; email: 21469228@qq.com (H. Li)

ABSTRACT

As a common agriculture waste as well as available biomass resource from ginkgo tree, ginkgo leaves were used as adsorbent to remove two models of cationic dyes methyl violet (MV) and malachite green (MG) after adequate modification. As the result, hydroxylated magnetic ginkgo leaf powder and carboxylated magnetic ginkgo leaf powder were obtained and characterized, respectively, which had the potential to be an environmentally friendly and economically effective biosorbents for the adsorption of dyes. These new biosorbents exhibited high adsorption capacity for dyes, with the maximum adsorption capacity of 450 mg g^{-1} for MV and 231 mg g^{-1} for MG. Further investigation confirmed that these adsorption processes were fitted with pseudo-second-order and Langmuir isothermal model. Moreover, these adsorbents with remarkable magnetism could be easily and rapidly recovered by external magnet after their use. The study demonstrated that the promising and reliable modified biosorbents were very suitable for removal of cationic dyes with high concentration at lower cost.

Keywords: Ginkgo leaves; Adsorption; Magnetic biosorbent; Dye removal; Modification

1. Introduction

Rapid industrialization contributes to significant improvement on economy, but it results in serious environmental pollution problems such as industrial wastewater, which has posed severe threat to human health [1]. Dye wastewater is one of major problem of industrial wastewater and is present in large amount in the wastewater from various types of industries such as paper, printing, textile, pharmaceutical, food, etc. [2]. Generally, synthetic dyes have impact on the light penetration and oxygen level in water [3]. The inadequate disposal of colored effluents, especially for dyes that have multiple benzene rings, can lead to the destruction of aquatic communities and cause various diseases because of toxic, mutagenic, and carcinogenic effect on live being [4–7]. Therefore, these residual organic dyes must be effectively removed before their disposal.

In order to handle the dye pollution, several techniques have been developed to for the treatment of colored wastewater, including adsorption, biodegradation, membrane filtration, electrochemical techniques, micellar enhanced ultrafiltration, and photocatalytic degradation [8–10]. Among them, adsorption process has been widely used as one of the effective, simple, and economical techniques for wastewater treatment [11]. Varieties of adsorbents such

* Corresponding authors.

as activated carbon [12], graphene oxides [13], gel [14], zeolites [15], metal-organic framework [16], clay minerals [17], and biosorbent from waste biomass [18], have been developed and tested as dye adsorbents. Recently, adsorbents derived from the biomass wastes like chitin [19], coffee grounds [20], pericarp [21], pectin [4], wheat straw [22], sugarcane bagasse [23], or peanut hull [24], have been paid more attention as the new class of adsorbents, not only for their significant reduction in the amount of waste produced but also for the great decrease in the cost of raw materials due to reasonable application of biological waste resources [25]. Fallen leaves, one of biomass wastes, are more widely distributed, abundant and easier to be collected than the above wastes, but most of them are disposed by landfill and incineration at present. Besides, relatively lower adsorption efficiency and longer separation time for dye solution have limited the practical application of the biomass adsorbents. Therefore, many chemical modification methods (e.g., acid, base, oxidant, and organic reagents treatment [26]) have used to promote raw biomass to have more abundant functional groups which can represent the binding sites to overcome its shortcoming in adsorption process. In addition, magnetically responsive modification procedure of biomass adsorbents is getting more attention because of more efficient and easier separation from dye solution [27].

Gingko tree, its nutlets used as traditional Chinese medicine, approach into city landscapes in most cities in China today [28]. There have been many researches on extracting the bioactive compounds of gingko leaves for recent years [29,30]. But a large number of fallen gingko leaves are not actually used, and instead as waste products in many cases [31]. Ginkgo leaves, a kind of agricultural wastes, they are rich in cellulose, hemicellulose, and lignin, and their surface contain a large number of functional groups such as hydroxyl, carbonyl, amino, carboxyl, and so on. These groups can adsorb organic compounds through hydrogen bonding, complexation and ion exchange, etc. [32]. Therefore, in order to make full use of this natural resource, gingko leaves with simple modification of organic reagents, endowed more hydroxyl, carbonyl groups and magnetism, were employed as adsorbent for the removal of two models of cationic dyes, methyl violet (MV) and malachite green (MG) in this paper. Batch adsorption experiments were conducted to evaluate factors affecting dye uptake, such as contact time, amount of adsorbents, initial dye concentration, pH and temperature. Besides, the adsorption mechanism and recyclability were investigated to show the adsorption characteristic of the novel adsorbent.

2. Materials and methods

2.1. Reagents

Glutaraldehyde, nano-sized ferroferric oxide (Fe_3O_4, 20 nm), glutamic acid and polyethylene glycol were purchased from Aladdin chemical reagent Co., Ltd., (Shanghai, China). Other reagents used were produced from Kelong Chemical Reagents Factory (Chengdu, China). All reagents were of analytical grade and all aqueous solutions were prepared with ultrapure water (18.25 MΩ cm) that was made in laboratory.

2.2. Preparation of hydroxylated magnetic ginkgo leaf powder

Fallen yellow ginkgo leaves were collected from the street trees of *Ginkgo biloba* in the Jiangan campus of Sichuan University at the end of October 2018. After their petioles were removed, ginkgo leaves (GL) were washed with pure water and dried at 50°C for 48 h. After grinding and sieving with 100 mesh sieve, particles of powder with size below 0.15 mm were obtained, denoted as GL, and stored in the dryer for later use. These preparation methods were based on the literature [33,34] with little modification. The schematic illustration for preparing hydroxylated magnetic ginkgo leaf powder (HMGL) and carboxylated magnetic ginkgo leaf powder (CMGL) is shown in supplemental file Fig. S1.

GL was stirred magnetically in 0.1 mol L^{-1} NaOH at 65°C for 4 h. After that, it was filtered and washed with ultrapure water for several times until the pH of the filtrate was neutral. Six grams of dried sample was put into a 100 mL Erlenmeyer flask containing 40 mL polyethylene glycol and was shaken at 25°C for 12 h. After the solvent in the mixture was removed, the solid was washed with ultrapure water for removing the residual solvent. Then, it was dispersed in 60 mL water containing 1.0 g Fe_3O_4 and was shaken at 25°C for 24 h. HMGL was obtained after being washed with water, separated by a magnet and dried at 50°C under vacuum.

2.3. Preparation of carboxylated magnetic ginkgo leaf powder

Six grams of GL treated with 0.1 mol L^{-1} NaOH at 65°C for 4 h was added to 15 mL of 50% glutaraldehyde solution. After shaking at 25°C for 12 h, 1.0 g of Fe_3O_4 was added and the mixture was shake for another 24 h. The solid was separated with a magnet and washed with water until the pH of the filtrate was around 7. After drying, the sample was added to an aqueous solution with pH of 10 containing 2 g glutamate and was shaken for 24 h. Then, CMGL were washed with water for several times with the aid of a magnet and dried in a vacuum oven at 50°C.

2.4. Characterization

Fourier transform infrared (FTIR) spectra of samples were recorded in the wavenumber region of 4,000–400 cm^{-1} with a spectrometer (two L1600300, PerkinElmer, USA). Their magnetic properties were determined using a superconducting quantum interference device (SQUID) (PPMS-9-VSM, Quantum Design, USA). Thermo gravimetric analysis was carried out with TG/DTA simultaneous measuring instrument (DTG-60(H), Shimadzu, Japan) under nitrogen. The microarchitecture of samples was characterized by scanning electron microscopy (SEM; TM3030, Kemei Analysis Instrument Co., Ltd., Changsha, China). X-ray diffraction (XRD) was performed by XRD6100 (Shimadzu, Japan) in the range of 5°–80°.

2.5. Dye adsorption experiments

The quantified adsorbent was placed into a 100 mL Erlenmeyer flask containing a known concentration dye

solution. Then the flask was put into an air-bath shaker (NRY-100C, Nanrong Laboratory Equipment Co., Ltd., Shanghai, China) at 200 rpm. After the adsorption, the adsorbent was separated from a solution by a magnet and the concentration of dye in liquid phase was determined at 580 and 619 nm for MV and MG by UV-vis spectrophotometer [15,35] (UV2800S, Shunyu Hengping Scientific Instrument Co., Ltd., Shanghai, China). The obtained linear regression equations were $y = 0.0558x - 0.058$ for MV and $y = 0.0317x - 0.0164$ for MG and these calibration curves showed a good correlation coefficient ($R^2 > 0.9990$). The adsorption tests were performed in four steps. Firstly, the effects of contact time, adsorbent dosage, pH, initial dye concentration, and temperature were investigated by batch experiment. The pH value of the solution was adjusted by 0.1 M HCl solution or NaOH solution. Secondly, in order to explore the effect of modification, the adsorption effect before and after modification were studied. Thirdly, kinetic curves and equilibrium isotherms were obtained to explore the adsorption mechanism. Finally, the repeated adsorption experiment of modified biomass waste was studied to investigate the reusable performance by the following method. The adsorbents HMGL and CMGL which had adsorbed dye were collected and dried. The adsorbent was eluted by shaking at 200 rpm in anhydrous ethanol solution for 4 h at 25°C. Then it was magnetically separated and washed with deionized water to neutral for reutilization. The potential of modified biomass wastes of ginkgo leaves to adsorb dye was evaluated by adsorption test as described in Fig. 1.

The adsorption of dye on modified biomass waste was evaluated with the adsorption rate (A, %) and equilibrium adsorption capacity (q_e, mg g^{-1}), which were calculated by Eqs. (1) and (2), respectively.

$$A = \frac{C_0 - C_e}{C_0} \times 100\%$$

(1)

$$q_e = \frac{(C_0 - C_e) \times V}{m}$$

(2)

where A is the adsorption rate (%), C_0 and C_e are the dye concentration before and after adsorption, respectively (mg L^{-1}), q_e is the amount of dye adsorbed at the equilibrium (mg g^{-1}), V is the total solution volume (L), and m is the mass of adsorbent (g).

The pseudo-first-order model and pseudo-second-order model were applied to analyze their adsorption kinetics. The kinetic models were shown in Eqs. (3) and (4), successively.

$$\log(q_e - q_t) = \log q_e - \frac{k_1 t}{2.303}$$

(3)

$$\frac{t}{q_t} = \frac{1}{k_2 q_e^2} + \frac{t}{q_e}$$

(4)

where k_1 is the pseudo-first-order rate constant (min^{-1}), q_t is the amount of adsorbate adsorbed at time (mg g^{-1}), t is the contact time (min), and k_2 is the pseudo-second-order rate constant (g mg^{-1}min^{-1}).

In this work, two equilibrium isotherm models, namely Freundlich and Langmuir were used as the model of adsorption isotherm in Eqs. (5) and (6) as followed, successively.

$$\ln q_e = \ln K_F + \frac{1}{n} \ln C_e$$

(5)

$$\frac{C_e}{q_e} = \frac{1}{K_L q_m} + \frac{C_e}{q_m}$$

(6)

where K_F is the Freundlich equilibrium constant ((mg g^{-1}) (L mg^{-1})$^{1/n}$), n is the heterogeneity factor, q_m is the maximum adsorption capacity of the adsorbent (mg g^{-1}), and K_L is the Langmuir equilibrium constant (L mg^{-1}).

2.6. Desorption and reusability experiments

To investigated the reusability of adsorbents for the adsorption of dyes, desorption experiments were carried out. Ethanol has been reported to be a good eluent for desorption of cationic dyes in some literatures [14,16,36]. Therefore, desorption experiments were performed by immersing adsorbents which adsorption capacity had reached equilibrium into ethanol as eluting agent. Regenerated adsorbents were collected by an external magnetic field, washed with eluting agent, and dried for the next cycle of dyes adsorption after the suspension was sonicated for 1 h. The concentration of dyes in the supernatant were measured by UV-vis spectrophotometer to obtain desorption percentage.

Fig. 1. Schematic illustration of the adsorption process.

The adsorption–desorption experiments were conducted for the successive five cycles.

3. Results and discussion

3.1. Characterization of the modified adsorbents

3.1.1. Morphological characterization

SEM images determined the surface morphology of GL, HMGL, and CMGL. As shown in Fig. 2a, the GL surface was rough, indicating that GL had the adsorption capacity. But the fibrous wall of the modified GL became thinner and exposed more fibrous structure, which was propitious for dye to the adsorption on the surface. It was obvious that the surface of CMGL was rougher than that of HMGL. This may be mainly related to the use of crosslinkers in the CMGL synthesis process. Furthermore, it could be seen that many small particles which were magnetic Fe_3O_4 nanoparticles adhered to the surface of HMGL and CMGL in Figs. $2a_2, a_3$.

3.1.2. Magnetic property analysis

Fig. 2b showed that magnetic hysteresis loops of HMGL and CMGL. From Fig. 1b, it could be seen that there were the *S*-like magnetic hysteresis loops in the magnetization curves of modified biomass, indicating the superparamagnetic behavior [37]. The saturation magnetic values of HMGL and CMGL were 5.35 and 7.67 emu g^{-1}, respectively. Compared to that of bare Fe_3O_4 nanoparticles [38], it was obvious that saturation magnetic value decreased after modification, which can be due to the formation of nonmagnetic organic substances covered Fe_3O_4 nanoparticles. CMGL exhibited larger magnetization intensity, which may be attribute to that more Fe_3O_4 nanoparticles were adhered to it. It could also be proved by thermogravimetric analysis. The inset of Fig. 2b shows that the adsorbents could be quickly separated and collected within 5 s from the aqueous solution with an external magnet due to their relatively strong magnetic intensity.

3.1.3. TG-DTG analysis

The TG-DTG curves of HMGL and CMGL were shown in Fig. 3a. Fe_3O_4 was stable within the range from 30°C to 800°C [38]. It can be seen that TG-DTG curves of HMGL and CMGL were similar, which was due to that these curves mainly reflected the thermogravimetric process of GL. The first weight loss occurred around 50°C –250°C, which was ascribed to the volatilization of the residue water and low molecules organic solvents. The second weight loss was mainly attributed to the degradation of cellulose and lignin in ginkgo leaves. From the curve of HMGL, the maximum decomposition rate was obtained at 332.71°C that was close to CMGL (325.41°C). The third weight loss presented the degradation of grafted organic molecules. According to TG, the residual amount of HMGL and CMGL were 24.56% and 38.01%, respectively. The reason may be that CMGL contains more ferric oxide, resulting in a larger residue
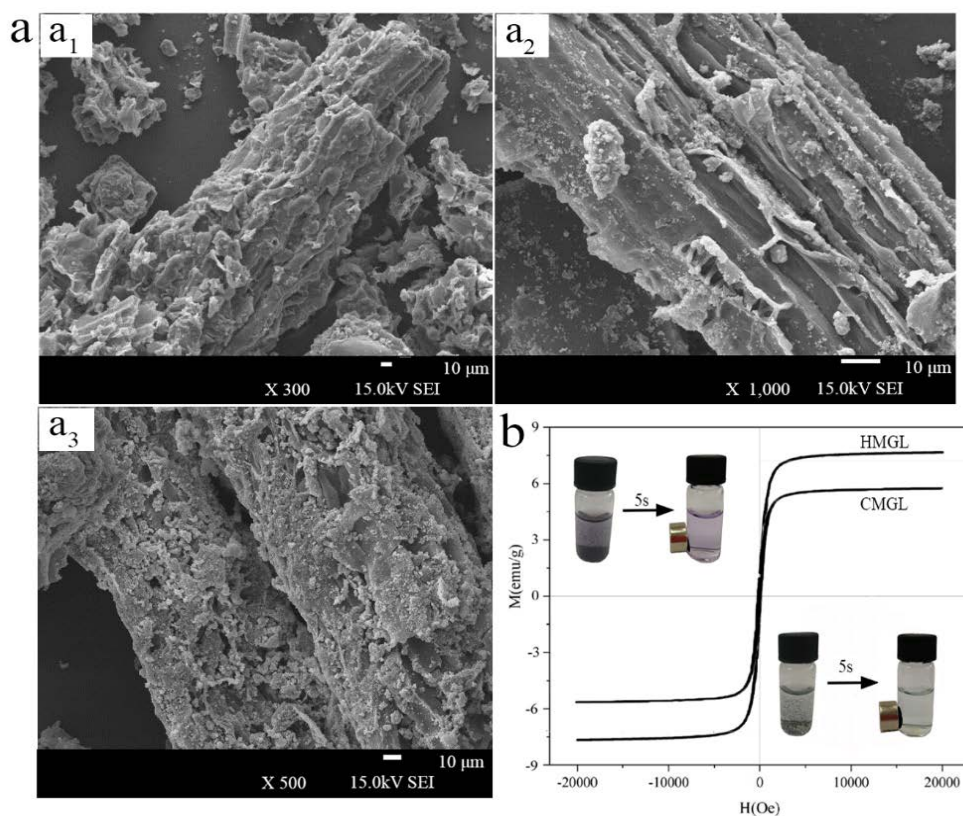
Fig. 2. SEM images (a) of GL (a_1), HMGL (a_2), and CMGL (a_3) and magnetization curves (b) of HMGL and CMGL.
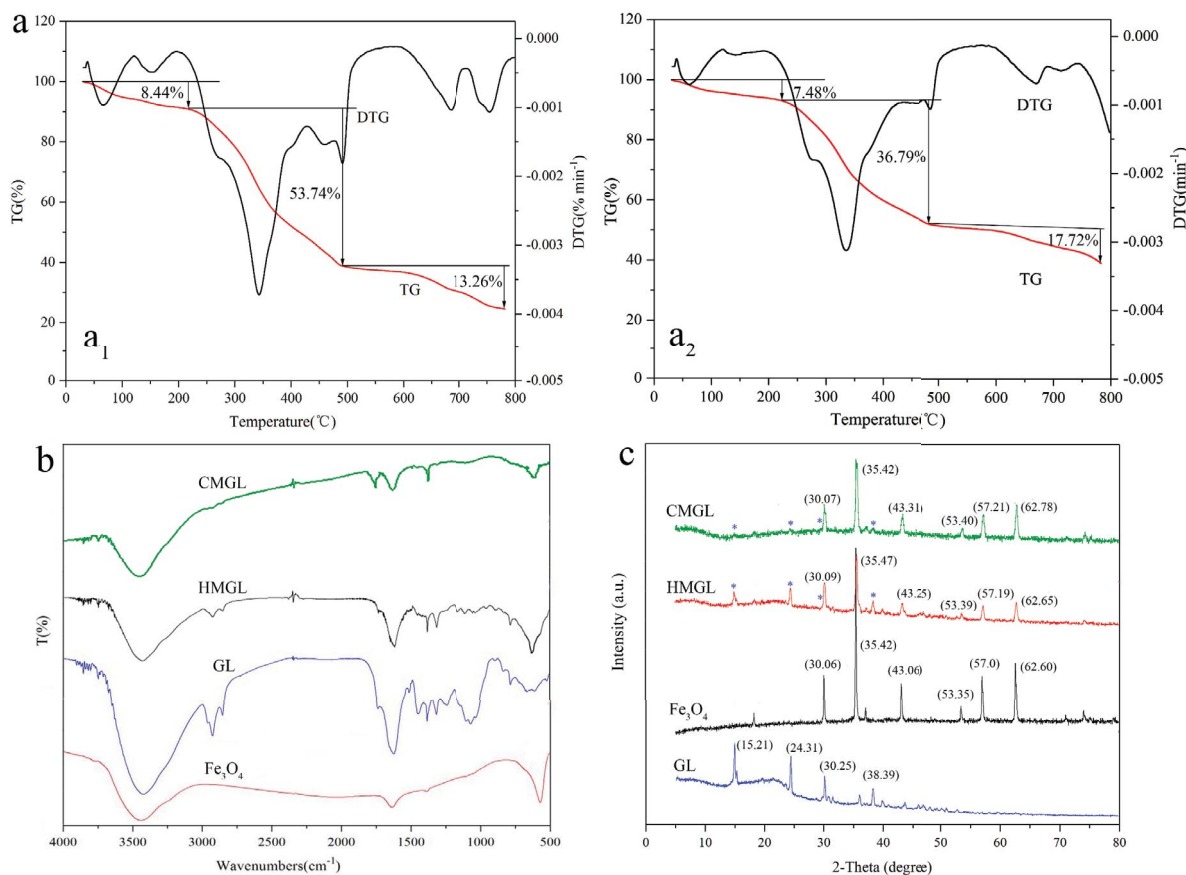
Fig. 3. TG-DTG curves (a) of HMGL(a_1) and CMGL(a_2), FTIR spectra (b) and X-ray diffraction patterns (c) of Fe_3O_4, GL, HMGL, and CMGL.

mass. Furthermore, the residual Fe_3O_4 can still be recovered after degradation of ineffective biomass adsorbents.

3.1.4. FITR analysis

The structures of Fe_3O_4, GL, HMGL, and CMGL were characterized by FTIR spectrum. In Fig. 3b, the peaks at 3,341 and 1,620 cm^{-1} represented stretching and bending vibration of O–H, respectively. which can be attributed to the components such as cellulose that contained hydroxyl group in ginkgo leaves [39]. Compared with the raw material GL, an absorption band at 580 cm^{-1} that was the characteristic peak of Fe_3O_4 and was generated by Fe–O stretching was shown in the spectra of HMGL and CMGL [40]. It was preliminarily proved that the modified GL had magnetic properties. In addition, the intensity of peak at 1,725 cm^{-1} related to carboxyl group was observed in the CMGL spectra, which could confirm the existence of carboxyl group introduced onto CMGL.

3.1.5. XRD analysis

The XRD patterns of Fe_3O_4, GL, HMGL, and CMGL were used to investigate their crystalline degree and were shown in Fig. 3c. The patterns of HMGL and CMGL presented the characteristic peaks of Fe_3O_4 occur at 2θ = 30.06°, 35.42°, 43.06°53.35°, 57.0°, and 62.60°, which was consistent with

the standard XRD data cards of Fe_3O_4 crystal (JCPDS no. 85–1436). This provided further evidence of magnetic properties of the modified materials. GL was observed to show several diffraction peaks at 2θ = 15.21°, 24.31°, 30.25°, and 38.39°, which correspond to the typical peaks of cellulose [41], and are also present in the XRD patterns of HMGL and CMGL.

3.2. Adsorption conditions of dyes on adsorbents

Batch adsorption experiments were conducted to explore the influence of adsorption conditions on the adsorption efficiency. Firstly, the effect of contact time was investigated at adsorbent dose of 0.04 g, 25°C, and initial concentration of 700 mg L^{-1} and the result was depicted in Fig. 4a. It was obvious that the adsorption rate was fast and the adsorption capacity rose rapidly in the first 30 min. The adsorption rate and the adsorption capacity reached the equilibrium after 40 min and were 90.04% and 450.20 mg g^{-1}, respectively. This rapid rate of adsorption could be attributed to large amount of active sites present on the surface of adsorbent at the initial stage of adsorption. Therefore, the adsorption rate and adsorption capacity attained steady state when the active sites were saturated.

Secondly, the influence of different adsorbent dosage on the adsorption efficiency was studied in Fig. 4b. It can be seen that the adsorption rate increased remarkably with
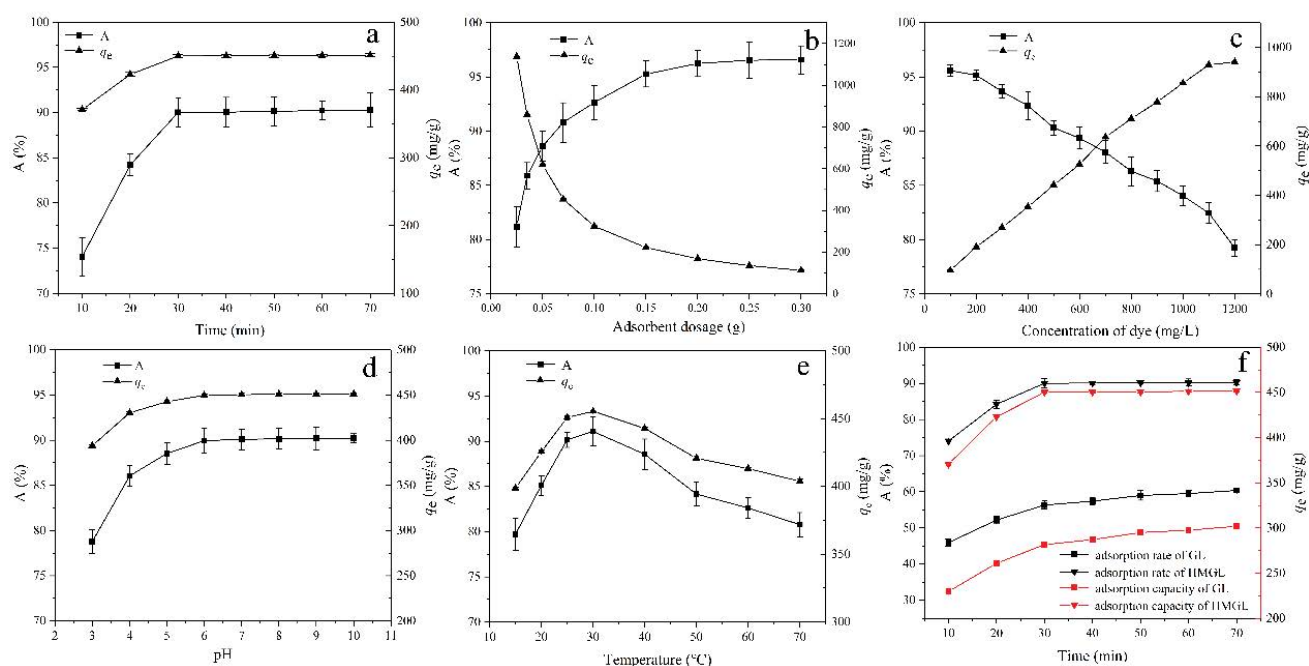
Fig. 4. Effects of contact time (a), adsorbent dosage (b), initial dye concentration (c), pH (d), temperature (e), and on MV adsorption with HMGL and comparison of adsorption rate and adsorption capacity of GL and HMGL (f).

increasing HMGL from 0.025 to 0.3 g, which could be attributable to more quantity of adsorption sites for the adsorption of MG. However, the decrease in adsorption capacity with the increase of adsorbent amount is due to the presence of unsaturated sites available on the surface of HMGL. Hence, the adsorption capacity changes in the opposite trend compared with the adsorption rate.

Then, Fig. 4c shows the effect of initial dye concentration (100–1,200 mg L^{-1}) on the adsorption efficiency. It was observed that adsorption rate was lower and adsorption capacity was higher with the increasing of the MV concentration. This result is in accordance with the previous reports [42,43]. High initial concentration can enhance the MV intermolecular interaction and weaken the interaction between MV and HMGL [42], which leads to the decrease of adsorption rate (A, %). On the contrary, the value of q_e can be higher when initial dye concentration increased, indicating that HMGL has great adsorption capacity for MV.

As known to all, pH value is very important for the adsorption process because of the influence on surface charge of adsorbents and degree of ionization of the adsorbate and is investigated with a range of values between 3.0 and 10.0 in increments of unity in this experiment. From Fig. 4d, it can be seen that adsorption rate and adsorption capacity increased as pH value increased from 3 to 7. When the pH value was higher than 7, the adsorption efficiency had no significant change. At low pH, H^+ may compete effectively with cationic MV for the available adsorption sites of adsorbent and the hydroxyl groups of HMGL becomes protonated, which can lead to the electrostatic repulsion between MV and HMGL to limit the performance of adsorbent [44]. During the experiment, pH value of MV aqueous solution under natural conditions was determined to be about 6–7.

The adsorption capacity of adsorbent reached the maximum, and its adsorption capacity was about 450 mg g^{-1} under this condition. The possibility of maximum dye removal without the alteration of solution pH adds to the favourability of the adsorbent.

Finally, the adsorption rate increased from 79.72% to 91.09%, and the adsorption capacity increased from 398 to 450 mg g^{-1} with rising temperature from 15°C to 30°C as shown in Fig. 4e, indicating that temperature had affected on the adsorption capacity. However, the adsorption capacity decreased at higher temperature, which indicated that the adsorption process could be exothermic. When the temperature increases, the mobility of dye molecules would be enhanced to undergo an interaction with active sites at the surface. Because of exothermic effect of dye adsorption, it is not conducive to remove the dye molecules from solution at higher temperature. The adsorption rate and capacity could remain at a high level at 25°C.

In order to verify the advantages of HMGL, the adsorption rate and capacity of GL and HMGL were compared and shown in Fig. 4f. The adsorption rate of HMGL was up to about 90% and the adsorption capacity was about 450 mg g^{-1}, which were nearly twice that of GL. More hydroxyl groups attached on the surface of HMGL would adsorb more dye molecules by electrostatic attraction, hydrogen bonding interaction, and conjugate action [42]. The maximum adsorption capacity of HMGL for MV adsorption and the other reported adsorbents in the literatures have been compared in Table 1. It can be seen that HMGL is better than the referenced adsorbents.

The adsorption parameter of contact time can be used to gauge the equilibrium time. As can be seen in Fig. 5a, its adsorption rate and adsorption capacity showed the same trend, both of which were gradually increased and tended

Table 1
Comparison of adsorption capability for MV and MG between modified biomass waste of ginkgo leaves and some of newly reported adsorbents in the literatures

Adsorbents	Dyes	q_e (mg g^{-1})	Reference
Cellulose filament/poly(NIPAM-co-AAc) hybridhydro gels	MV	226.02	[47]
Chitin derived biochar	MV	30.58	[19]
Microbial salecan polysaccharide-based gels	MV	178.9	[45]
Hyper-branched polyglycerol based multi-carboxylic magnetic gel	MV	400	[14]
Ginkgo leaf powder	MV	294.4	In this study
Hydroxylated magnetic ginkgo leaf powder	MV	450	In this study
Mangifera indica seed kernel powder	MG	22.8	[48]
Zeolite nanostructures from waste aluminum cans (ZF)	MG	226.75	[15]
Magnetic activated carbon	MG	217.68	[49]
Polycatechol modified Fe$_3$O$_4$ magnetic nanoparticles	MG	66.84	[50]
Copper sulfide nanorods loaded on activated carbon	MG	145.98	[51]
Corncob particles modified with phosphoric acid	MG	148	[52]
Ginkgo leaf powder	MG	188.9	In this study
Carboxylated magnetic ginkgo leaf powder	MG	231	In this study

to equilibrium in 120 min at the initial dye concentration of 300 mg L^{-1}, adsorbent dose of 0.025 g, pH value of 6 and 25°C. Therefore, the contact time was controlled at 120 min in the next experiments.

The effect of amount of CMGL are presented in Fig. 5b. Obviously, the results of adsorption rate and adsorption capacity were consistent with these of HMGL. The adsorption rate (*A*, %) was improved significantly with increasing amount of CMGL because of more adsorption sites. Conversely, the value of q_e gradually decreased, which was

due to that the number of dye molecules attached to per unit adsorbent was reduced.

The dye removal for different initial dye concentrations were shown in Fig. 5c. Because of the high ratio of active binding sites to the number of MV molecules, the high removal rate achieved at low dye concentrations. However, with the concentration of solution from 400 to 900 mg L^{-1}, the adsorption rate decreased rapidly. It is related to the saturation of sorption sites on the surface of the adsorbent. Moreover, the adsorption capacity increased, which could be
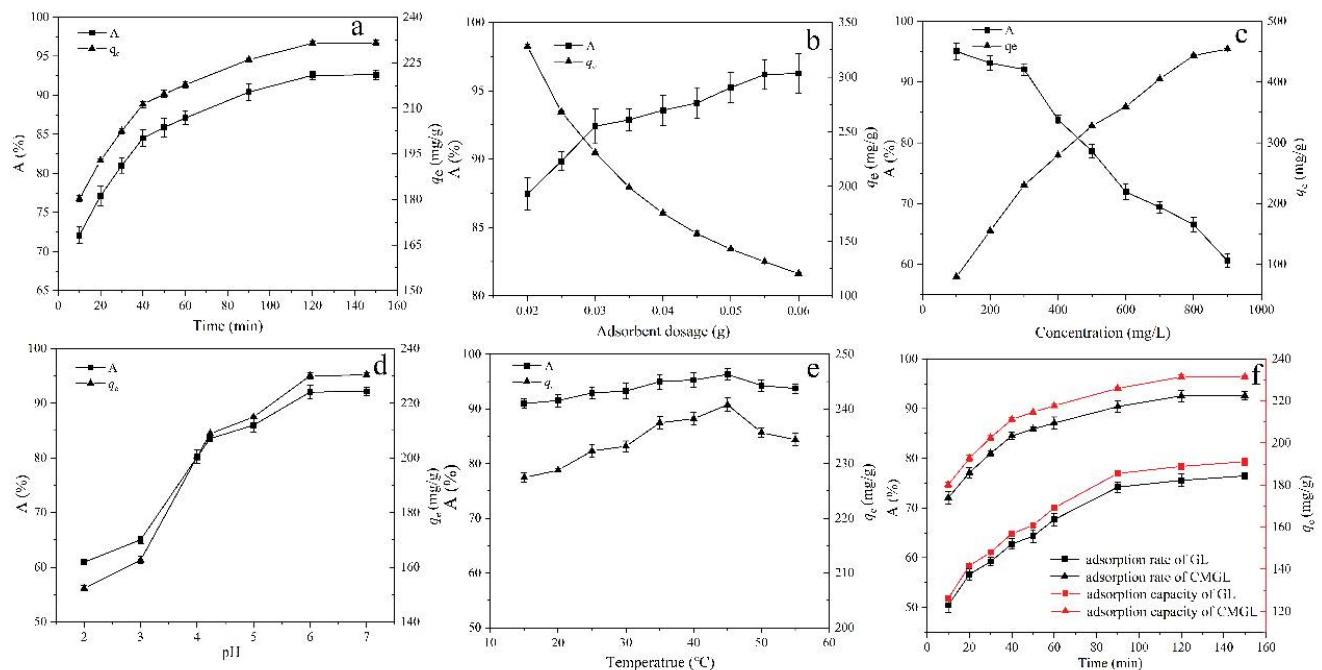
Fig. 5. Effect of contact time (a), adsorbent dosage (b), initial dye concentration (c), pH (d), temperature (e), and on MG adsorption with CMGL and comparison of adsorption rate and adsorption capacity of GL and CMGL (f).

as a result of the high driving force for mass transfer at higher initial dye concentrations.

Similarly, the effect of pH on the uptake of MG was investigated by changing the pH value of dye solution from 2 to 7 in Fig. 5d. It was observed that the adsorption rate of MG increased from 60.72% to 90.02%, and the adsorption capacity increased from 152.31 to 230.07 mg g⁻¹ with the increasing of pH value from 2 to 6, then became steady. The reason is similar to the adsorption of HMGL on MV. The adsorption sites of CMGL are competed with MG molecules by excess of hydrogen ions at low pH environment because MG is also a cationic dye [6].

Moreover, Fig. 5e showed the effect of temperature at range of 15°C–55°C. The adsorption rate and adsorption capacity slightly changed with rising temperature, indicating that the temperature had less effect on the adsorption process. The adsorption rate and capacity were 92.92% and 231.31 mg g⁻¹ at 25°C, which were at a high level. Thus, in order to simplify the operation and save energy, the adsorption experiments were conducted at room temperature.

In order to evaluate the effect of the modified GL on the MG adsorption, the results of MG removal on GL and CMGL were presented and compared in Fig. 5f. Compared with GL, the adsorption rate and adsorptive capacity of CMGL were greatly increased. The adsorption rate of CMGL was faster than that of GL at the same time. The maximum adsorption rate and adsorption capacity of GL were 76% and 191.12 mg g⁻¹, respectively, thus that of CMGL were about 92.55% and 231 mg g⁻¹. The reason is that CMGL had more carboxyl groups on the surface than GL so that the adsorption effect has been greatly improved. Furthermore,

compared to other adsorbents in Table 1, the CMGL is superior to those reported results for MG adsorption.

3.3. Adsorption kinetics and adsorption isotherm of dyes on adsorbents

The adsorption kinetics of the dyes on HMGL were represented in Fig. 6a and were analyzed and correlated to the pseudo-first-order kinetic (Fig. 6b) and pseudo-second-order kinetic models (Fig. 6c). The adsorption equilibrium of MV on HMGL was reached within 40 min for high dye concentration of 700 mg L⁻¹ under natural condition. It has shorter contact time than those reported results under a high amount of dye concentration [17,45]. The fitting parameters are summarized in Table 2. It is obvious that R^2 of pseudo-second-order kinetic model is greater and the experimental values ($q_{e,\exp}$) is closer to calculated values ($q_{e,cal}$), indicating that pseudo-second-order kinetic model is better in describing the adsorption of MV. The fact demonstrated that the adsorption process was controlled by chemical adsorption mechanism, which suggested electronic sharing or electron transfer between HMGL and MV [43].

Adsorption isotherm curves are critical to describe the relationship between the dye molecules interacting with adsorbent under certain temperature. Fig. 6d shows the adsorption isotherms of MV at 25°C, 30°C, and 40°C. It was observed that the equilibrium adsorption capacity increased with the increasing equilibrium concentration until adsorption saturation. The most widely used Langmuir isotherm (Fig. 6e) and Freundlich isotherms (Fig. 6f) were employed
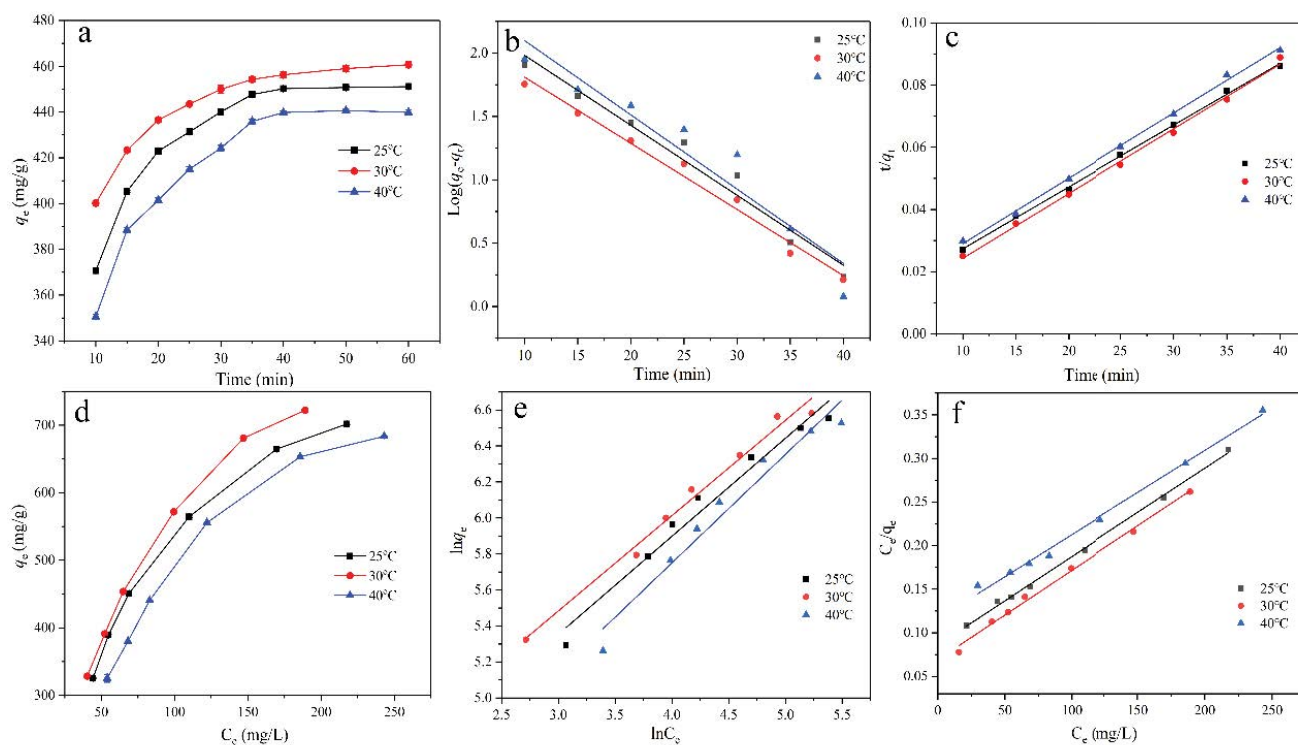
Fig. 6. Adsorption kinetics curve of MV (a), pseudo-first-order model (b), pseudo-second-order model (c), the adsorption isotherms of MV (d), Freundlich isotherms linearized model (e), and Langmuir isotherms linearized model (f).

Table 2
Parameters of two kinetic models for MV adsorption on HMGL

T (°C)	$q_{e,\exp}$ (mg g^{-1})	Pseudo-first-order			Pseudo-second-order		
		$q_{e,\text{cal}}$ (mg g^{-1})	k_1 (min^{-1})	R^2	$q_{e,\text{cal}}$ (mg g^{-1})	k_2 (g (mg min)$^{-1}$)	R^2
25	450.91	342.08	0.1272	0.9683	473.93	0.0244	0.9986
30	456.89	214.91	0.1203	0.9853	502.51	0.0388	0.9969
40	439.98	483.34	0.1350	0.9199	454.55	0.0232	0.9981

for fitting the experimental data. According to larger the correlation coefficients R^2 shown in Table 3, it is clear that Langmuir isotherm is more ideal for the adsorption isotherms of MV, suggesting the monolayer sorption of dye adsorption on HMGL [43].

Adsorption isotherm curves are critical to describe the relationship between the dye molecules interacting with adsorbent under certain temperature. Fig. 5d shows the adsorption isotherms of MV at 25°C, 30°C, and 40°C. It was observed that the equilibrium adsorption capacity increased with the increasing equilibrium concentration until adsorption saturation. The most widely used Langmuir isotherm (Fig. 5e) and Freundlich isotherms (Fig. 5f) were employed for fitting the experimental data. According to larger the correlation coefficients R^2 shown in Table 3, it is clear that Langmuir isotherm is more ideal for the adsorption isotherms of MV, suggesting the monolayer sorption of dye adsorption on HMGL [43].

The adsorption kinetic curves for MG were obtained at three different temperatures (25°C, 35°C, and 45°C) are shown in Fig. 7a to explore the mechanism. The adsorption equilibrium of MG on CMGL was established after about 120 min for dye concentration of 300 mg L^{-1} at pH of 6. It took longer time to reach equilibrium compared to some literature [36,46]. But the dye concentration in our experiment of the adsorption kinetic is higher than that of these literatures. In the solution of higher concentration, equilibrium reached slower because of the weaker adsorption driving forces as compared to the dye solutions of lower concentration. The pseudo-first-order (Fig. 7b) and pseudo-second-order (Fig. 7c) kinetic models are employed to fit the adsorption kinetic data. The relevant adsorption parameters are listed in Table 4, and the pseudo-second-order model can express well the adsorption kinetic data because of the higher correlation coefficients (R^2) and negligible differences between the experimental values ($q_{e,\exp}$) and the calculated values ($q_{e,\text{cal}}$). It indicates that chemical adsorption plays a significant role in MG removal [17].

Adsorption isotherm curves are shown in Fig. 6d. Similarly, the Freundlich and Langmuir models were also employed to fit the adsorption isotherms, as shown in Figs. 6e,f and Table 5. The experimental data fitted much better with Langmuir model ($R^2 > 0.991$) than Freundlich model ($R^2 < 0.987$) for all the tested temperatures. The phenomenon suggests that the adsorption process is monolayer adsorption of MG molecules from aqueous solution to the surface.

3.4. Recycling performance of the modified GL adsorbents for removal of dye molecules

For the practical applications, the stability and reusability of the adsorbents are related to the cost-effectiveness of the adsorbents [16]. The reusability of HMGL and CMGL were investigated up to the fifth run via regeneration of used adsorbents by washing with ethanol and are shown in Figs. 8a and b, respectively. The desorption percentage were 90.2% and 94.6% for MV and MG dyes by using ethanol as an eluting agent in desorption experiment. The reusability experiments of HMGL for MV adsorption were carried out at the initial dye concentration of 700 mg L^{-1}, adsorbent dosage of 0.07 g, and contact time of 40 min at room temperature. As shown in Fig. 8a, the adsorption capacity of adsorbent HMGL decreased gradually. The main explanation is that the dye molecules adsorbed on the HMGL cannot be completely eluted after washing with ethanol. Residual dye molecules have occupied the active sites on the adsorbent surface, which lead to that fresh MV cannot be adsorbed. Moreover, the initial dye concentration used in this experiment is too high, which can promote a rapid decline in adsorption capacity with the number of recycles. HMGL can be recycled twice at high initial dye concentration. The reusability experiment of CMGL for MG adsorption showed a similar result with MV adsorption experiment at the initial dye concentration of 300 mg L^{-1}, adsorbent dosage of 0.03 g, and contact time of 120 min at room temperature.

Table 3
Parameters of two isotherm models for MV adsorption on HMGL

T (°C)	Freundlich			Langmuir		
	n	K_F (min^{-1})	R^2	$q_{e,\text{cal}}$ (mg g^{-1})	K_L (g (min^{-1})$^{-1}$)	R^2
25	1.8374	41.3032	0.9712	502.51	0.0232	0.9981
30	1.8891	49.1747	0.9865	561.79	0.0258	0.9952
40	1.6589	28.1819	0.9599	480.77	0.0179	0.9940
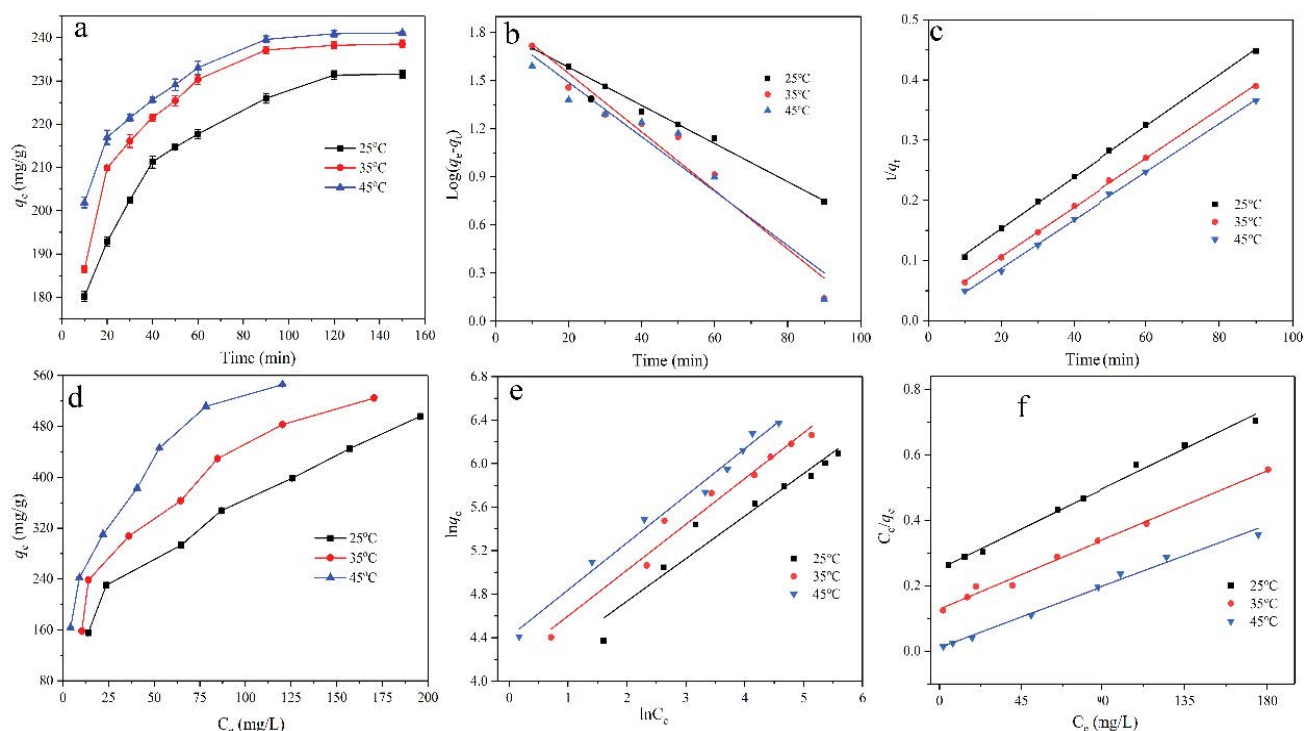
Fig. 7. Adsorption kinetics curve of MG (a), pseudo-first-order model (b), pseudo-second-order model (c), the adsorption isotherms of MG (d), Freundlich isotherms linearized model (e), and Langmuir isotherms linearized model (f).

Table 4
Parameters of two kinetic models for MG adsorption on CMGL

T (°C)	$q_{e,\exp}$ (mg g^{-1})	Pseudo-first-order			Pseudo-second-order		
		$q_{e,\mathrm{cal}}$ (mg g^{-1})	k_1 (min^{-1})	R^2	$q_{e,\mathrm{cal}}$ (mg g^{-1})	k_2 (g (mg min)$^{-1}$)	R^2
25	231.38	66.26	0.0274	0.9855	234.74	0.0164	0.9994
35	238.23	81.36	0.0420	0.9571	245.09	0.0259	0.9995
45	241.12	67.44	0.0391	0.9283	250.01	0.0477	0.9992

But adsorbent capacity of CMGL for MG decreased more slowly, which could be attribute to MG adsorbed on CMGL was more easily eluted in ethanol solutions. CMGL could be reused at least up to three times with high adsorption efficiency.

4. Conclusions

In the present research, abundant waste fallen ginkgo leaves had been modified simply and employed as adsorbents for the removal of MG and MV dyes from aqueous solutions. Modified ginkgo leaf powder presented many advantages in the adsorption process. Firstly, biomass waste is cost-effective and can lead to green chemistry process based on the energy consumption and environmental impact. Then adsorbents can be separated easily and quickly from dye solution with magnet. Moreover, the magnetization showed a synergistic dye adsorption because of more polarity of Fe–O in magnetite [4]. Above

all, modified biomass adsorbent with the abundance of hydroxyl or carboxyl groups exhibits satisfactory adsorption capacity for MG (450 mg g^{-1}) and MV (231 mg g^{-1}), which were higher than raw material and most of the newly reported adsorbent. In addition, the adsorption process of MG or MV can both be well described by Langmuir isotherm model and pseudo-second-order kinetic model, indicating that it is a monolayer chemical adsorption process. Modified biosorbents exhibited remarkable effect on the adsorption of MV and MG at high initial dye concentration, thereby proposing an efficient and inexpensive adsorbent alternative for removal of dye pollutants with a great application prospect in the wastewater treatment.
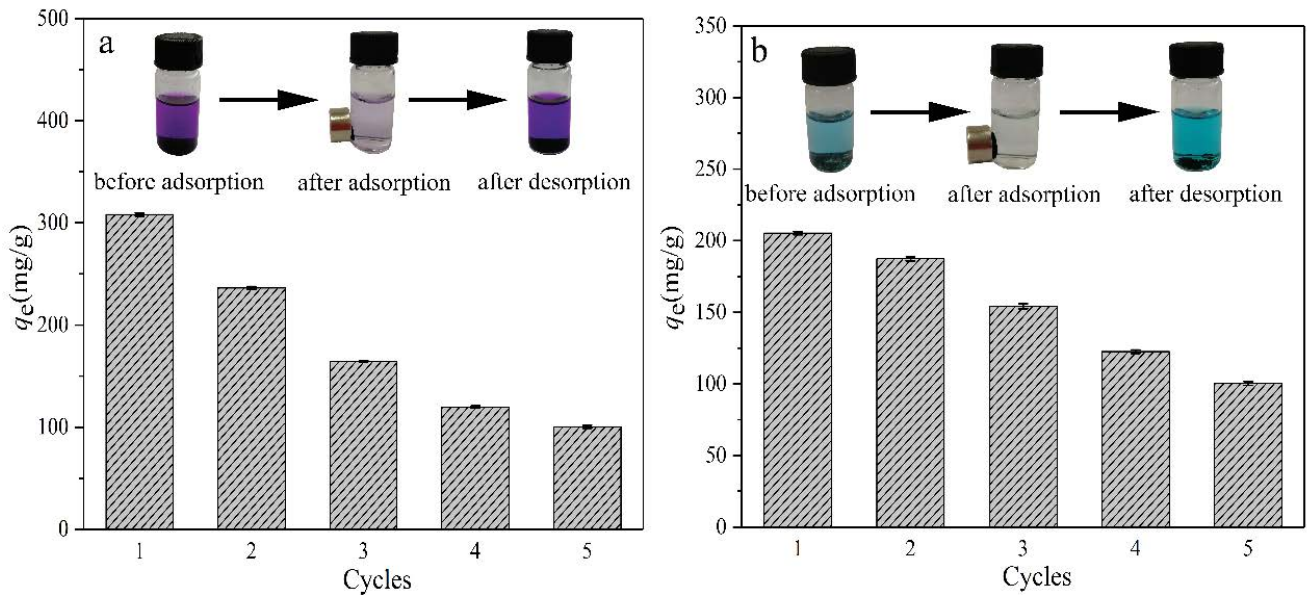
Fig. 8. Reusability of HMGL for MV adsorption (a) and CMGL for MG adsorption (b) and the changing process before and after adsorption.

Table 5
Parameters of two isotherm models for MG adsorption on CMGL

	Freundlich			Langmuir		
T (°C)	n	K_F (min^{-1})	R^2	$q_{e,cal}$ (mg g^{-1})	K_L (g (min^{-1})$^{-1}$)	R^2
25	2.5570	52.0852	0.9481	361.01	0.0110	0.9938
35	2.3760	65.3509	0.9756	425.53	0.0183	0.9913
45	2.3127	81.9755	0.9865	480.76	0.1801	0.9916

Symbols

A	—	Adsorption rate, %
q_e	—	Amount of dye adsorbed at the equilibrium, mg g^{-1}
C_0	—	Initial dye concentration, mg L^{-1}
C_e	—	Dye concentration after the batch adsorption procedure, mg L^{-1}
V	—	The total solution volume, L
m	—	Mass of adsorbent, g
k_1	—	The pseudo-first-order rate constant, min^{-1}
q_t	—	Amount of adsorbate adsorbed at time, mg g^{-1}
t	—	Contact time, min
k_2	—	The pseudo-second-order rate constant, g mg^{-1}min^{-1}
K_F	—	Freundlich equilibrium constant, (mg g^{-1}) (L mg^{-1})$^{1/n}$
n	—	Heterogeneity factor
q_m	—	Maximum adsorption capacity of the adsorbent, mg g^{-1}
K_L	—	Langmuir equilibrium constant, L mg^{-1}

References

[1] X.Z. Jiang, P.P. Sun, L. Xu, Y.R. Xue, H. Zhang, W.C. Zhu, *Platanus orientalis* leaves based hierarchical porous carbon microspheres as high efficiency adsorbents for organic dyes removal, Chin. J. Chem. Eng., 28 (2020) 254–265.

[2] A.N. Módenes, F.R. Espinoza-Quiñones, C.A.Q. Geraldi, D.R. Manenti, D.E.G. Trigueros, A.P.d. Oliveira, C.E. Borba, A.D. Kroumov, Assessment of the banana pseudostem as a low-cost biosorbent for the removal of reactive blue 5G dye, Environ. Technol., 36 (2015) 2892–2902.

[3] T.S. Kazeem, S.A. Lateef, S.A. Ganiyu, M. Qamaruddin, A. Tanimu, K.O. Sulaiman, S.M. Sajid Jillani, K. Alhooshani, Aluminium-modified activated carbon as efficient adsorbent for cleaning of cationic dye in wastewater, J. Cleaner Prod., 205 (2018) 303–312.

[4] A.C. Khorasani, S.A. Shojaosadati, Magnetic pectin-*Chlorella vulgaris* biosorbent for the adsorption of dyes, J. Environ. Chem. Eng., 7 (2019), doi: 10.1016/j.jece.2019.103062.

[5] N.B. Singh, G. Nagpal, S. Agrawal, Rachna, Water purification by using adsorbents: a review, Environ. Technol. Innovation, 11 (2018) 187–240.

[6] M.S. Ma, Z. Liu, L.F. Hui, Z. Shang, S.Y. Yuan, L. Dai, P.T. Liu, X.L. Liu, Y.H. Ni, Lignin-containing cellulose nanocrystals/ sodium alginate beads as highly effective adsorbents for cationic organic dyes, Int. J. Biol. Macromol., 139 (2019) 640–646.

[7] L.J. Xia, A.M. Wang, C.H. Zhang, Y. Liu, H. Guo, C.L. Ding, Y.L. Wang, W.L. Xu, Environmentally friendly dyeing of cotton in an ethanol–water mixture with excellent exhaustion, Green Chem., 20 (2018) 4473–4483.

[8] M. Ali, Q. Husain, N. Alam, M. Ahmad, Nano-peroxidase fabrication on cation exchanger nanocomposite: augmenting catalytic efficiency and stability for the decolorization and detoxification of Methyl Violet 6B dye, Sep. Purif. Technol., 203 (2018) 20–28.

[9] M. Vinayagam, S. Ramachandran, V. Ramya, A. Sivasamy, Photocatalytic degradation of orange G dye using ZnO/biomass activated carbon nanocomposite, J. Environ. Chem. Eng., 6 (2018) 3726–3734.

[10] K. Samal, C. Das, K. Mohanty, Application of saponin biosurfactant and its recovery in the MEUF process for removal of methyl violet from wastewater, J. Environ. Manage., 203 (2017) 8–16.

[11] L.J. Xia, C. Li, S.J. Zhou, Z. Fu, Y. Wang, P. Lyu, J.J. Zhang, X. Liu, C.H. Zhang, W.L. Xu, Utilization of waste leather powders for highly effective removal of dyes from water, Polymers, 11 (2019), doi: 10.3390/polym11111786.

[12] Y.H. Hao, Z. Wang, Z.M. Wang, Y.J. He, Preparation of hierarchically porous carbon from cellulose as highly efficient adsorbent for the removal of organic dyes from aqueous solutions, Ecotoxicol. Environ. Saf., 168 (2019) 298–303.

[13] G. Abdi, A. Alizadeh, J. Amirian, S. Rezaei, G. Sharma, Polyamine-modified magnetic graphene oxide surface: feasible adsorbent for removal of dyes, J. Mol. Liq., 289 (2019), doi: 10.1016/j.molliq.2019.111118.

[14] Y. Song, Y. Duan, L. Zhou, Multi-carboxylic magnetic gel from hyperbranched polyglycerol formed by thiol-ene photopolymerization for efficient and selective adsorption of methylene blue and methyl violet dyes, J. Colloid Interface Sci., 529 (2018) 139–149.

[15] E.A. Abdelrahman, Synthesis of zeolite nanostructures from waste aluminum cans for efficient removal of malachite green dye from aqueous media, J. Mol. Liq., 253 (2018) 72–82.

[16] M. Sarker, S. Shin, J.H. Jeong, S.H. Jhung, Mesoporous metal-organic framework PCN-222(Fe): promising adsorbent for removal of big anionic and cationic dyes from water, Chem. Eng. J., 371 (2019) 252–259.

[17] J. Tang, L. Zong, B. Mu, Y.F. Zhu, A.Q. Wang, Preparation and cyclic utilization assessment of palygorskite/carbon composites for sustainable efficient removal of methyl violet, Appl. Clay Sci., 161 (2018) 317–325.

[18] J.G. Wu, T. Zhang, C.Y. Chen, L.Y. Feng, X.H. Su, L.X. Zhou, Y.Y. Chen, A.Q. Xia, X.F. Wang, Spent substrate of *Ganodorma lucidum* as a new bio-adsorbent for adsorption of three typical dyes, Bioresour. Technol., 266 (2018) 134–138.

[19] M.A. Zazycki, P.A. Borba, R.N.F. Silva, E.C. Peres, D. Perondi, G.C. Collazzo, G.L. Dotto, Chitin derived biochar as an alternative adsorbent to treat colored effluents containing methyl violet dye, Adv. Powder Technol., 30 (2019) 1494–1503.

[20] X. Wen, H.S. Liu, L. Zhang, J. Zhang, C. Fu, X.Z. Shi, X.C. Chen, E. Mijowska, M.J. Chen, D.Y. Wang, Large-scale converting waste coffee grounds into functional carbon materials as high-efficient adsorbent for organic dyes, Bioresour. Technol., 272 (2019) 92–98.

[21] K. Samal, N. Raj, K. Mohanty, Saponin extracted waste biomass of *Sapindus mukorossi* for adsorption of methyl violet dye in aqueous system, Surf. Interfaces, 14 (2019) 166–174.

[22] Q.W. Lin, K.W. Wang, M.F. Gao, Y.S. Bai, L. Chen, H.Z. Ma, Effectively removal of cationic and anionic dyes by pH-sensitive amphoteric adsorbent derived from agricultural waste-wheat straw, J. Taiwan Inst. Chem. Eng., 76 (2017) 65–72.

[23] N.M. Noor, R. Othman, N.M. Mubarak, E.C. Abdullah, Agricultural biomass-derived magnetic adsorbents: preparation and application for heavy metals removal, J. Taiwan Inst. Chem. Eng., 78 (2017) 168–177.

[24] N. Tahir, H.N. Bhatti, M. Iqbal, S. Noreen, Biopolymers composites with peanut hull waste biomass and application for Crystal Violet adsorption, Int. J. Biol. Macromol., 94 (2017) 210–220.

[25] W.Y. Jiang, L.Y. Zhang, X.M. Guo, M. Yang, Y.W. Lu, Y.J. Wang, Y.S. Zheng, G.T. Wei, Adsorption of cationic dye from water using an iron oxide/activated carbon magnetic composites prepared

[26] from sugarcane bagasse by microwave method, Environ. Technol., (2019), doi: 10.1080/09593330.2019.1627425.

[26] L. Bulgariu, L.B. Escudero, O.S. Bello, M. Iqbal, J. Nisar, K.A. Adegoke, F. Alakhras, M. Kornaros, I. Anastopoulos, The utilization of leaf-based adsorbents for dyes removal: a review, J. Mol. Liq., 276 (2019) 728–747.

[27] R. Angelova, E. Baldikova, K. Pospiskova, Z. Maderova, M. Safarikova, I. Safarik, Magnetically modified *Sargassum horneri* biomass as an adsorbent for organic dye removal, J. Cleaner Prod., 137 (2016) 189–194.

[28] K. Zou, X.D. Liu, D. Zhang, Q. Yang, S.D. Fu, D.L. Meng, W.Q. Chang, R. Li, H.Q. Yin, Y.L. Liang, Flavonoid biosynthesis is likely more susceptible to elevation and tree age than other branch pathways involved in phenylpropanoid biosynthesis in ginkgo leaves, Front. Plant Sci., 10 (2019), doi: 10.3389/fpls.2019.00983.

[29] F.P. Wang, W.M. Zhang, X.H. Tan, Z.B. Wang, Y.X. Li, W. Li, Extract of *Ginkgo biloba* leaves mediated biosynthesis of catalytically active and recyclable silver nanoparticles, Colloids Surf., A, 563 (2019) 31–36.

[30] C.W. Zhang, C.Z. Wang, R. Tao, J.Z. Ye, Separation of polyprenols from *Ginkgo biloba* leaves by a nano silica-based adsorbent containing silver ions, J. Chromatogr., A, 1590 (2019) 58–64.

[31] Z. Wang, L. Chen, Adsorption characteristics of dibutyl phthalate from aqueous solution using ginkgo leaves-activated carbon by chemical activation with zinc chloride, Desal. Water Treat., 54 (2014) 1969–1980.

[32] Y.B. Zhou, J. Lu, Y. Zhou, Y.D. Liu, Recent advances for dyes removal using novel adsorbents: a review, Environ. Pollut., 252 (2019) 352–365.

[33] Z.K. Wang, S.L. Zhang, H.Y. Chen, M. Jiang, Z.W. Zhou, Preparation of magnetic polyethyleneimine functionalized rice straw and its adsorption properties for Pb(II) ions, Res. Environ. Sci., 30 (2017) 1316–1324.

[34] D. Cheng, Y.B. Wen, L.J. Wang, X.Y. An, X.H. Zhu, Y.H. Ni, Adsorption of polyethylene glycol (PEG) onto cellulose nano-crystals to improve its dispersity, Carbohydr. Polym., 123 (2015) 157–163.

[35] A.I. Abd-Elhamid, H.F. Aly, H.A.M. Soliman, A.A. El-Shanshory, Graphene oxide: follow the oxidation mechanism and its application in water treatment, J. Mol. Liq., 265 (2018) 226–237.

[36] E. Boorboor Azimi, A. Badiei, J.B. Ghasemi, Efficient removal of malachite green from wastewater by using boron-doped mesoporous carbon nitride, Appl. Surf. Sci., 469 (2019) 236–245.

[37] P.F. Chen, H. Song, S. Yao, X.Y. Tu, M. Su, L. Zhou, Magnetic targeted nanoparticles based on β-cyclodextrin and chitosan for hydrophobic drug delivery and a study of their mechanism, RSC Adv., 7 (2017) 29025–29034.

[38] P.F. Chen, H. Song, L. Zhou, J. Chen, J.Y. Liu, S. Yao, Magnetic solid-phase extraction based on ferroferric oxide nanoparticles doubly coated with chitosan and β-cyclodextrin in layer-by-layer mode for the separation of ibuprofen, RSC Adv., 6 (2016) 56240–56248.

[39] R. Kumar, R.K. Sharma, Synthesis and characterization of cellulose based adsorbents for removal of Ni(II), Cu(II) and Pb(II) ions from aqueous solutions, React. Funct. Polym., 140 (2019) 82–92.

[40] A.I.A. Sherlala, A.A.A. Raman, M.M. Bello, A. Buthiyappan, Adsorption of arsenic using chitosan magnetic graphene oxide nanocomposite, J. Environ. Manage., 246 (2019) 547–556.

[41] X.F. Ma, C.Z. Liu, D.P. Anderson, P.R. Chang, Porous cellulose spheres: preparation, modification and adsorption properties, Chemosphere, 165 (2016) 399–408.

[42] W. Zhang, X.T. Feng, Y. Alula, S. Yao, Bionic multi-tentacled ionic liquid-modified silica gel for adsorption and separation of polyphenols from green tea (*Camellia sinensis*) leaves, Food Chem., 230 (2017) 637–648.

[43] L.R. Nie, J. Lu, W. Zhang, A. He, S. Yao, Ionic liquid-modified silica gel as adsorbents for adsorption and separation of water-soluble phenolic acids from *Salvia militiorrhiza* bunge, Sep. Purif. Technol., 155 (2015) 2–12.

[44] L.R. Bonetto, F. Ferrarini, C. de Marco, J.S. Crespo, R. Guégan, M. Giovanela, Removal of methyl violet 2B dye from aqueous solution using a magnetic composite as an adsorbent, J. Water Process Eng., 6 (2015) 11–20.

[45] X.L. Qi, Z.P. Li, L.L. Shen, T. Qin, Y.N. Qian, S.Z. Zhao, M.C. Liu, Q.K. Zeng, J.J. Shen, Highly efficient dye decontamination via microbial salecan polysaccharide-based gels, Carbohydr. Polym., 219 (2019) 1–11.

[46] E. Sharifpour, E. Alipanahpour Dil, A. Asfaram, M. Ghaedi, A. Goudarzi, Optimizing adsorptive removal of malachite green and methyl orange dyes from simulated wastewater by Mn-doped CuO-nanoparticles loaded on activated carbon using CCD-RSM: mechanism, regeneration, isotherm, kinetic, and thermodynamic studies, Appl. Organomet. Chem., 33 (2019), doi: 10.1002/aoc.4768.

[47] M. Zhang, Y. Li, Q.L. Yang, L.L. Huang, L.H. Chen, H.N. Xiao, Adsorption of methyl violet using pH- and temperature-sensitive cellulose filament/poly(NIPAM-co-AAc) hybrid hydrogels, J. Mater. Sci., 53 (2018) 11837–11854.

[48] D. Singh, V. Sowmya, S. Abinandan, S. Shanthakumar, Removal of malachite green dye by *Mangifera indica* seed kernel powder, J. Inst. Eng. (India) Ser. A, 99 (2017) 103–111.

[49] E. Altintig, M. Onaran, A. Sarı, H. Altundag, M. Tuzen, Preparation, characterization and evaluation of bio-based magnetic activated carbon for effective adsorption of malachite green from aqueous solution, Mater. Chem. Phys., 220 (2018) 313–321.

[50] Y.N. Hua, J. Xiao, Q.Q. Zhang, C. Cui, C. Wang, Facile synthesis of surface-functionalized magnetic nanocomposites for effectively selective adsorption of cationic dyes, Nanoscale Res. Lett., 13 (2018), doi: 10.1186/s11671-018-2476-7.

[51] E. Sharifpour, H.Z. Khafri, M. Ghaedi, A. Asfaram, R. Jannesar, Isotherms and kinetic study of ultrasound-assisted adsorption of malachite green and Pb^{2+} ions from aqueous samples by copper sulfide nanorods loaded on activated carbon: experimental design optimization, Ultrason. Sonochem., 40 (2018) 373–382.

[52] H.W. Hu, W.X. Liang, Y.Y. Zhang, S.Y. Wu, Q.N. Yang, Y.B. Wang, M. Zhang, Q.J. Liu, Multipurpose use of a corncob biomass for the production of polysaccharides and the fabrication of a biosorbent, ACS Sustainable Chem. Eng., 6 (2018) 3830–3839.

Supplementary information
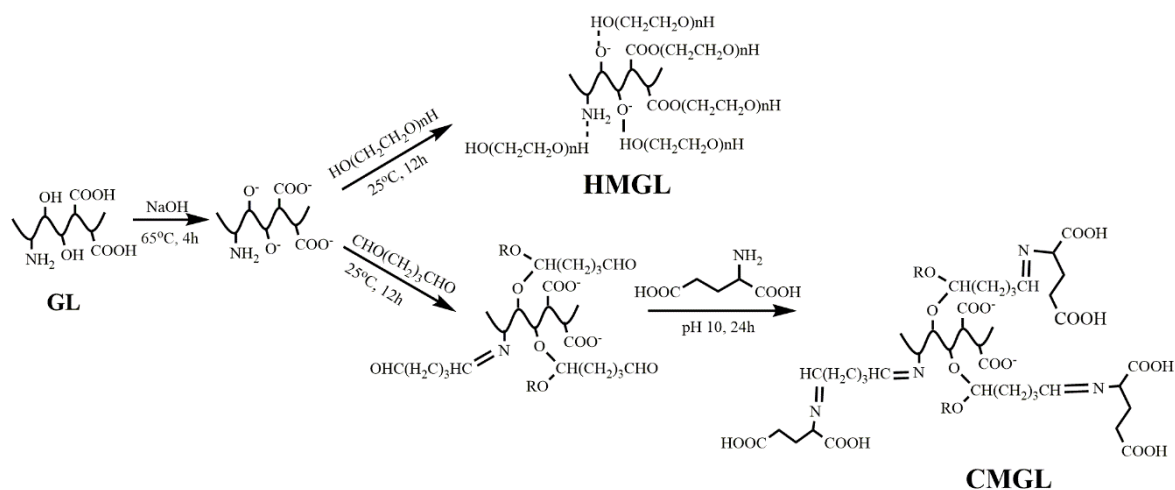
Fig. S1. Schematic illustration for preparing HMGL and CMGL.